

Dirac spectra and edge states in honeycomb plasmonic lattices

Dezhuan Han,¹ Yun Lai,¹ Jian Zi,² Zhao-Qing Zhang,¹ and C. T. Chan¹

¹*Department of Physics, Hong Kong University of Science and Technology, Clear Water Bay, Kowloon, Hong Kong, China*

²*Department of Physics, Fudan University, Shanghai 200433, People's Republic of China*

(Dated: September 14, 2021)

We study theoretically the dispersion of plasmonic honeycomb lattices and find Dirac spectra for both dipole and quadrupole modes. Zigzag edge states derived from Dirac points are found in ribbons of these honeycomb plasmonic lattices. The zigzag edge states for out-of-plane dipole modes are closely analogous to the electronic ones in graphene nanoribbons. The edge states for in-plane dipole modes and quadrupole modes, however, have rather unique characters due to the vector nature of the plasmonic excitations. The conditions for the existence of plasmonic edge states are derived analytically.

PACS numbers: 42.70.Qs, 41.20.Jb, 73.20.Mf

Metal nanoparticles support remarkable optical resonances known as localized surface plasmons [1, 2]. Surface plasmons are collective electronic density waves bound at metal surfaces that can locally enhance incident optical fields by orders of magnitude. The enhanced optical fields in the near field give rise to many extraordinary optical phenomena such as surface-enhanced Raman scattering [3, 4] and single-molecule fluorescence detection [5]. The arrangement of metal nanoparticles regularly can offer more. It has been shown that a chain of closely spaced metal nanoparticles can guide electromagnetic (EM) energy with lateral mode confinement below the diffraction limit [6]. Two-dimensional (2D) lattices consisting of metal nanoparticles show interesting tunable optical response over the entire visible range [7]. A three-dimensional arrangement of metal nanoparticles can form metallic photonic crystals (PCs) with robust photonic band gaps that depend on the local order rather than on the symmetry or the global long range order [8]. Metal nanoparticles thus manifest promising building blocks for plasmonic materials, leading to unprecedented applications in nanophotonics, nonlinear optics, bio-sensing, and even medical therapy.

Recently, graphene has received considerable interest because of the existence of the Dirac point that offers remarkable electronic properties [9, 10, 11]. The Dirac spectra in 2D PCs for EM waves have also been identified [12, 13] and the Dirac-point-derived edge states have novel transportation properties when time-reversal symmetry breaking is introduced. These edge states can render "one-way" waveguiding for EM waves, confirmed by numerical simulations [14]. Both graphene and 2D PCs support Dirac dispersions. However, the Dirac spectrum in graphene is derived directly from the nearest-neighbor hopping of bound electron states, while that in 2D PCs corresponds to the photonic bands of scattering photons.

In this paper, we study theoretically the plasmonic band structures of metal nanospheres arranged in a honeycomb lattice. The plasmonic lattice is an open system that supports both guided modes and leaky modes [15],

and as such, it is different from electronic graphene and 2D PCs. Furthermore, the Dirac dispersions found in graphene and 2D PCs are only for scalar waves. The 2D plasmonic lattice can support both scalar waves and vector waves. Our results reveal that for both scalar and vector waves, this honeycomb plasmonic lattice possesses Dirac points for the infinite system and guided edge states when an edge is present. The existence of Dirac points and edge states in plasmonic systems may open up new avenues in both physics and applications for the emerging field of plasmonics.

The honeycomb plasmonic structure under study is shown in Fig. 1(a), in which each black dot in the $x-y$ plane represents a metal sphere. Its Brillouin zone (BZ) is shown Fig. 1(b). The inter-distance between adjacent spheres is $a_0 = a/\sqrt{3}$, where a is the lattice constant. The primitive and reciprocal lattice vectors are, respectively, given by $\mathbf{a}_{1,2} = a(\pm 1/2, \sqrt{3}/2)$ and $\mathbf{b}_{1,2} = 2\pi(\pm 1, 1/\sqrt{3})/a$. We use the Drude-type permittivity $\varepsilon(\omega) = 1 - \omega_p^2/\omega^2$ with $\omega_p = 6.18$ eV for metal spheres. The lattice constant is chosen to be $a = 60$ nm, and the sphere radius is $r_s = 10$ nm. For this ratio $r_s/a = \sqrt{3}/6$, the dipole and quadrupole dispersions are separated in energy as demonstrated below.

The plasmonic dipole dispersions calculated within the quasi-static approximation (QSA) limit are shown in Fig. 1(c), in which the red dots are for out-of-plane \mathbf{P}_{out} modes and the black dots correspond to in-plane \mathbf{P}_{in} modes. The \mathbf{P}_{in} and \mathbf{P}_{out} modes form their own orthogonal subspaces. We see that there are two Dirac cones at the K point, one for the \mathbf{P}_{in} and one for the \mathbf{P}_{out} modes. Fig. 1(d) shows the plasmonic dispersions in the QSA limit if only quadrupoles (\mathbf{Q}) are considered. We found a Dirac point at about 3.9 eV, which is the single sphere quadrupole resonance frequency. At these Dirac points, the constant frequency surfaces are represented by two cones meeting at the K point. It should be pointed out that the in-plane dipole and quadrupole modes are vector waves in nature. The existence of Dirac dispersions in these cases is a result of the symmetry of the honeycomb

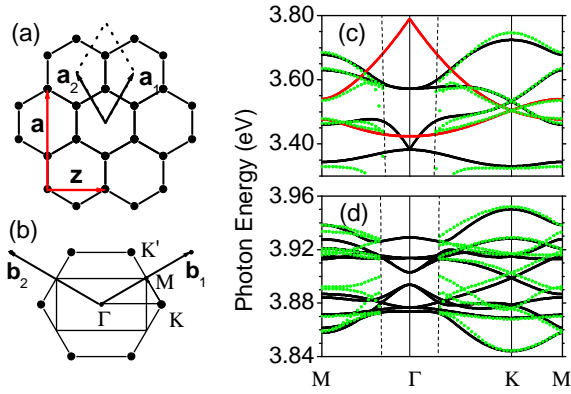


FIG. 1: (Color online) (a) Schematic structure of the honeycomb plasmonic lattice. \mathbf{a}_1 , \mathbf{a}_2 are the primitive vectors; \mathbf{a} and \mathbf{z} are the 1D primitive vectors for armchair and zigzag ribbons respectively. (b) Reciprocal lattice vectors. (c) QSA band structures for in-plane dipole modes (black dots) and out-of-plane dipole modes (red dots); (d) QSA band structures for quadrupoles. MST results (electrodynamics calculation with retardation effects taken fully into account) are also shown in (c) and (d) by green dots. The dashed lines in panels (c) and (d) indicate the light lines. The lattice constant is 60 nm and the sphere radius is 10 nm.

structure which is robust against their vector nature.

We note that the l -th multipole plasmon resonance frequency of a small plasmonic sphere is $\omega_l = [l/(2l+1)]^{1/2} \omega_p$. When the spheres are arranged in a lattice, each multipole resonance couples to form a set of bands, and these manifolds do not mix when r_s/a_0 is small. The dipole and quadrupole bands shown in Fig. 1 are indeed separated in energy. In Figs. 1(c) and (d), we compare the QSA results with the fully fledged multiple scattering theory (MST) results (shown in green color) [16]. The MST gives a solution to Maxwell equations that takes into account the full retardation effects. The comparison between the MST (green dots) and QSA results is shown in Fig. 1(c) for dipole modes and in Fig. 1(d) for quadrupole modes. The details of the MST method are described elsewhere [16]. The MST dispersions are shown only for $k > \omega/c$, since the leaky modes inside the light cone are not well defined due to the coupling with free photons. As the K point is far away from light cone, the Dirac dispersion found by QSA agrees well with the MST calculations. We will discuss the Dirac dispersions with QSA since it can give a more straightforward interpretation.

An important consequence of the Dirac spectrum in graphene electronics is the existence of peculiar edge states [11] with unusual physical properties [10] in graphene ribbons with finite widths. Two types of graphene nanoribbons, namely armchair and zigzag ribbons, are usually considered. In Fig. 1(a), the vector \mathbf{a} (\mathbf{z}) indicates the translation vector of the armchair (zigzag) ribbons, and the shorter (longer) side of the rect-

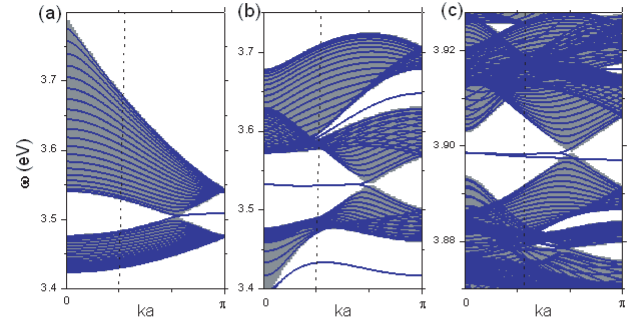


FIG. 2: (Color online) Band structures for $N = 20$ zigzag plasmonic ribbons (blue) and projected bands for the 2D honeycomb structure along the corresponding reciprocal axis (grey area). (a) Out-of-plane dipole modes. The flat band between $2\pi/3$ and π corresponds to edge states. (b) In-plane dipole modes. The flat band with ka ranging from 0 to $2\pi/3$ corresponds to Dirac-point-derived edge states. (c) Quadrupole modes. Near the single particle resonance 3.9 eV ($\omega_{l=2}$), there are two additional bands: one with ka ranging from 0 to $2\pi/3$, the other traversing the whole BZ. The system parameters are the same as in Fig. 1.

angle inside the 2D graphene BZ is the 1D BZ of the armchair (zigzag) ribbons. The band structure of the armchair (zigzag) graphene ribbons can be predicted by the projection of 2D graphene bands onto the corresponding axis of the reciprocal lattice vector. The original Dirac point K (K') is expected to appear at $ka = 0$ ($2\pi/3$) for armchair (zigzag) ribbons. Compared with the projected 2D electronic graphene bands, a new feature of zigzag ribbons is the appearance of edge states that extends from $ka = \pi$ to $2\pi/3$, where $ka = 2\pi/3$ is the expected degeneracy point of the 2D projected graphene bands. These new additional edge states form a flat band at energy $E = 0$ with wave functions localized near the edge sites. Within a tight-binding model, the necessary condition for $E = 0$ edge states is "zero-hopping", namely, the total sum of hopping terms over the nearest neighbor sites should vanish. For a semi-infinite graphene sheet with a zigzag edge, the tight-binding model shows that when $ka = \pi$, the edge state wave function is completely localized. Thereafter the decay length becomes longer and smoothly connects to a delocalized state at $ka = 2\pi/3$, which is the 2D graphene Dirac point.

We now discuss the Dirac-point-derived edge states of plasmonic ribbons. Unless otherwise stated, the results for finite-width plasmonic ribbons here are calculated for $N = 20$ zigzag and armchair ribbons, where N is an integer characterizing the width of the ribbon [11]. We expect that the edge states of out-of-plane modes might be similar to those of electronic edge states derived from the out-of-plane π states in graphene, while the edge states for the \mathbf{P}_{in} and \mathbf{Q} modes (if there are any) might be very different. We note that electronic graphene [11] and 2D PCs studied recently [13] are all

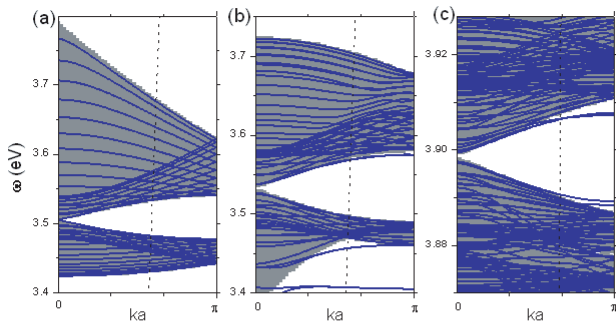


FIG. 3: (Color online) Same as Fig. 2 but for armchair plasmonic ribbons. There is no edge state for the armchair ribbon near the single particle resonance at 3.52 eV (dipole) or 3.9 eV (quadrupole).

dealing with scalar waves. In their cases, the electron and photon transport near the Dirac points can be described by the "two-component" massless Dirac Hamiltonian $\mathbf{H} = \gamma(k_x\sigma_x + k_y\sigma_y)$, where γ is a band parameter and σ is the Pauli matrix. In the plasmonic sphere arrays, the vector nature of EM waves enters explicitly, and the underlying physics can go beyond the "two-component" Dirac equation.

In Fig. 2, the blue dots represent the plasmonic bands of zigzag ribbons for out-of-plane dipole, in-plane dipole and quadrupole. The bands are superimposed on top of the plasmonic bands of the 2D honeycomb lattice projected along the zigzag axis, which are shown as the grey background. For \mathbf{P}_{out} modes in Fig. 2(a), we see that the ribbon bands basically overlap the projected 2D bands with the exception of an additional degenerate flat band starting from about $ka = 2\pi/3$ to π in the gap of the projected bands, which corresponds to the edge states in the zigzag graphene ribbons. This flat band occurs at 3.51 eV (the single sphere dipole resonance $\omega_{l=1} = 3.52$ eV), which has the similar physical meaning of $E = 0$ ("zero-hopping") in graphene. The slight differences in the edge state frequencies and $\omega_{l=1}$ come from the hopping among farther sites in the lattice, which is neglected in the tight-binding model for graphene.

For \mathbf{P}_{in} modes, there is no edge state from $ka = 2\pi/3$ to π , however, a new additional flat band with its frequency near $\omega_{l=1}$ emerges from $ka = 0$ to about $2\pi/3$. This phenomenon is rather different from that in the zigzag graphene ribbon, where the edge states are forbidden near the Γ point. The "two-component" effective Dirac equation commonly used in graphene electronics is not valid in this case since the vector nature of EM waves introduces extra degrees of freedom. More interesting observation can be made when we come to quadrupoles. Two sets of edge states appear near the single particle resonance at $\omega_{l=2} = 3.9$ eV. The dispersion of one set of edge states is similar to the in-plane dipole edge mode discussed above, as it is almost flat and is confined between

$0 \leq ka < 2\pi/3$. There is an additional band of edge states with a small and negative group velocity that goes all the way from $ka = 0$ to π .

The \mathbf{P}_{out} , \mathbf{P}_{in} and \mathbf{Q} modes for the armchair plasmonic ribbons are shown in Fig. 3 as blue dots, overlaid on top of the 2D plasmonic bands (grey color) projected along the armchair axis. There is no additional flat band near the single sphere resonance $\omega_{l=1}$ for dipoles or $\omega_{l=2}$ for quadrupoles. We can thus conclude that the Dirac-point-derived edge states observed in the plasmonic system come from the boundary condition (zigzag edge) which is analogous to that in electronic graphene.

In the following, we give an analytic derivation of the condition for the existence of plasmonic zigzag edge states near multipole resonance frequencies by truncating the Green function to the nearest neighbor. Let us consider a general tensor field \mathbf{F} of rank l (which can be the electric field in the case of a dipole or the field gradient in the case of a quadrupole) generated by a localized source \mathbf{V} with rank l (dipole, quadrupole...). In free space, the field and the source are related by the $2l$ -th rank Green function $\mathbf{G}(\mathbf{r} - \mathbf{r}')$ which satisfies $\mathbf{F}(\mathbf{r}) = \mathbf{G}(\mathbf{r} - \mathbf{r}')\mathbf{V}(\mathbf{r}')$ and the linear response gives $\mathbf{V}(\mathbf{r}) = \alpha\mathbf{F}(\mathbf{r})$, where α is the multipole polarizability. We place these point sources \mathbf{V} on a semi-infinite honeycomb lattice with a zigzag edge as shown in the inset of Fig. 4. The indices (m, n) in the inset are used to label the honeycomb sites, where n and m label the position along (or y -axis) and perpendicular to (x -axis) the zigzag chain respectively (see Fig. 4). $\mathbf{r}_{m,n}$ is the coordinate of the (m, n) site, and the site $(1, n + 1/2)$, located between $(1, n)$ and $(1, n + 1)$, is chosen to be the origin for convenience. We search for eigenstates with a Bloch wavevector k along the zigzag edge and we demand that the frequency should be equal to the single particle multipole resonance frequency. If we truncate the Green function to the nearest neighbor, the condition for the frequency to be equal to the single particle multipole resonance frequency is "zero-hopping", namely a zero sum of the fields from the three nearest neighbors. This gives

$$\mathbf{G}(-\mathbf{r}_{1,n})\mathbf{V}_{1,n} + \mathbf{G}(-\mathbf{r}_{1,n+1})\mathbf{V}_{1,n+1} + \mathbf{G}(-\mathbf{r}_{2,n+\frac{1}{2}})\mathbf{V}_{2,n+\frac{1}{2}} = 0, \quad (1)$$

where $\mathbf{V}_{m,n} = \mathbf{V}_m e^{in ka}$ if the periodic Bloch condition is imposed. From Eq. (1) a matrix \mathbf{T} relating \mathbf{V}_1 and \mathbf{V}_2 can be defined as

$$\mathbf{T} = -\mathbf{G}^{-1}(-\mathbf{r}_{2,n+\frac{1}{2}})[\mathbf{G}(-\mathbf{r}_{1,n})e^{-ika/2} + \mathbf{G}(-\mathbf{r}_{1,n+1})e^{ika/2}]. \quad (2)$$

This procedure can be done iteratively to obtain $\mathbf{V}_m = \mathbf{T}^{m-1}\mathbf{V}_1$. The eigenvalues of the matrix \mathbf{T} give the properties of the states. If $|\lambda| < 1$, the states are localized edge states, while $|\lambda| = 1$ corresponds to a Bloch state extending to the interior of the ribbon.

For out-of-plane modes, the Green function $\mathbf{G}^{P_{out}}(\mathbf{r} - \mathbf{r}')$ is just an isotropic scalar function and Eq. (1) is

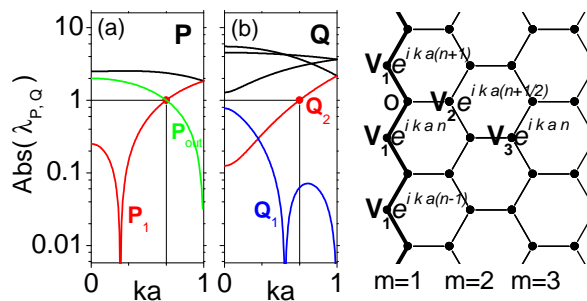


FIG. 4: (Color online) Absolute values of eigenvalues λ of the matrix \mathbf{T} as a function of the Bloch wavevector k . \mathbf{V} is either \mathbf{P} or \mathbf{Q} . $|\lambda| < 1$ gives the condition for edge states. (a) Dipole modes. The green line is for out-of-plane modes and the red and black lines are for in-plane modes. (b) Quadrupole modes. \mathbf{Q}_1 (blue) is always an edge state, while \mathbf{P}_1 and \mathbf{Q}_2 give edge state solutions when $ka < 2\pi/3$. The inset is a sketch of a semi-infinite honeycomb structure with a zigzag edge. The indices (m, n) and vector wave functions are defined as shown.

reduced to $p_{z1}e^{inka} + p_{z1}e^{i(n+1)ka} + p_{z2}e^{i(n+\frac{1}{2})ka} = 0$, which is exactly the same condition found for electronic graphene [11]. This is why the edge state behavior of the out-of-plane mode is so similar to that of electronic graphene ribbons. The ratio p_{z2}/p_{z1} is simply given by $-2\cos ka$ and is shown by green lines in Fig. 4(a). For the in-plane dipole mode, the QSA dyadic dipolar Green function can be written as $\mathbf{G}^{pin}(\mathbf{r} - \mathbf{r}')\mathbf{P}_{in}(\mathbf{r}') = [3(\mathbf{n} \cdot \mathbf{P}_{in})\mathbf{n} - \mathbf{P}_{in}]/|\mathbf{r} - \mathbf{r}'|^3$, where \mathbf{n} is the unit vector along the $\mathbf{r} - \mathbf{r}'$ direction, and \mathbf{T} is a 2×2 matrix that can be found analytically. In Fig. 4(a), the absolute values of the two eigenvalues are plotted by red and black lines. The black curve is always larger than 1, while the red curve is smaller than 1 when $ka < 2\pi/3$, denoted as \mathbf{P}_1 in the figure, which explains why in-plane dipolar edge states are confined by $0 \leq ka < 2\pi/3$. For quadrupoles, there are five independent variables $\{Q_{yy}, Q_{zz}, Q_{xy}, Q_{xz}, Q_{yz}\}$ and the corresponding QSA Green function can be derived analytically after tedious algebra. The details will be published elsewhere. \mathbf{T} -matrix becomes a 5×5 matrix, and the absolute values of the five eigenvalues are plotted in Fig. 4(b). Only two sets of eigenvalues give absolute values less than 1 and thus form edge states. The edge state solution labeled as \mathbf{Q}_1 (blue) is smaller than unity in the whole 1D BZ. This corroborates the existence of an edge state band that goes from $ka = 0$ to π in Fig. 2(c) in the $N = 20$ zigzag plasmonic ribbon. Another state denoted by \mathbf{Q}_2 (red) has a critical value for the edge state at $ka = 2\pi/3$ similar to the in-plane dipole mode \mathbf{P}_1 .

Another interesting observation that can be deduced from Fig. 4 is that the eigenvalues for the \mathbf{T} -matrix go to zero at $ka = 0.26\pi$ and 0.54π for \mathbf{P}_1 and \mathbf{Q}_1 respectively, which implies that the corresponding edge states are localized at the edge completely. In contrast, com-

pletely localized states in electronic graphene are only found at the BZ boundary $ka = \pi$. The completely localized state away from the BZ boundary comes from the vector nature of EM waves.

In summary, we have found Dirac spectra in "graphene-like" plasmonic structures for both dipole and quadrupole coupling. Edge states for plasmonic lattices with finite widths are also identified and analyzed numerically and their existence conditions are derived analytically. The edge states for the out-of-plane dipole modes in zigzag plasmonic ribbons resemble those of the electronic graphene zigzag edge states, but the edge states for in-plane dipole and quadrupole modes have rather unique characters due to their vector nature. These results can lead to the study of Dirac point behavior in yet another class of interesting material.

This work was supported by the Central Allocation Grant from the Hong Kong RGC through HKUST3/06C. Computation resources were supported by the Shun Hing Education and Charity Fund. We thank Drs. Xianyu Ao and Kin Hung Fung for helpful discussions.

-
- [1] U. Kreibig and M. Vollmer, *Optical Properties of Metal Clusters* (Springer, New York, 1995).
 - [2] S. A. Maier, *Plasmonics: Fundamentals and Applications* (Springer, New York, 2007).
 - [3] S. Nie and S. R. Emory, *Science* **275**, 1102 (1997).
 - [4] K. Kneipp, *et al.*, *Phys. Rev. Lett.* **78**, 1667 (1997).
 - [5] P. Anger, P. Bharadwaj, and L. Novotny, *Phys. Rev. Lett.* **96**, 113002 (2006).
 - [6] S. A. Maier, *et al.*, *Nat. Mater.* **2**, 229 (2003).
 - [7] A. Tao, P. Sinsersuksakul, and P. D. Yang, *Nature Nano.* **2**, 435 (2007).
 - [8] W. Y. Zhang, *et al.*, *Phys. Rev. Lett.* **84**, 2853 (2000).
 - [9] K. S. Novoselov, *et al.*, *Science* **306**, 666 (2004).
 - [10] Y. W. Son, M. L. Cohen, and S. G. Louie, *Nature (London)* **444**, 347 (2006).
 - [11] K. Nakada, M. Fujita, G. Dresselhaus, and M. S. Dresselhaus, *Phys. Rev. B* **54**, 17954 (1996).
 - [12] M. Plihal, and A. A. Maradudin, *Phys. Rev. B* **44**, 8565 (1991).
 - [13] F. D. M. Haldane and S. Raghu, *Phys. Rev. Lett.* **100**, 013904 (2008).
 - [14] Z. Wang, Y. D. Chong, J. D. Joannopoulos, and M. Soljacic, *Phys. Rev. Lett.* **100**, 013905 (2008).
 - [15] S. Y. Park and D. Stroud, *Phys. Rev. B* **69**, 125418 (2004); W. H. Weber and G. W. Ford, *Phys. Rev. B* **70**, 125429 (2004); D. S. Citrin, *Nano Lett.* **4**, 1561 (2004); A. Alu and N. Engheta, *Phys. Rev. B* **74**, 205436 (2006); A. F. Koenderink and A. Polman, *Phys. Rev. B* **74**, 033402 (2006); V. A. Markel and A. K. Sarychev, *Phys. Rev. B* **75**, 085426 (2007).
 - [16] K. H. Fung and C. T. Chan, *Opt. Lett.* **32**, 973 (2007); Y. R. Zhen, K. H. Fung, and C. T. Chan, *Phys. Rev. B* **78**, 035419 (2008).